PCCP

Accepted Manuscript

ROYAL SOCIETY OF CHEMISTRY

www.rsc.org/pccp

PCCP

RSCPublishing

PERSPECTIVE

Nanostructured Carbon-Based Cathode Catalysts for Nonaqueous Lithium-Oxygen Batteries

Cite this: DOI: 10.1039/x0xx00000x

Qing Li,[a] Ruiguo Cao,[b] Jaephil Cho,[b,*] and Gang Wu[a,*]

Received 00th January 2012,
Accepted 00th January 2012

DOI: 10.1039/x0xx00000x

www.rsc.org/

Although lithium-ion batteries are traditionally considered to be the most promising candidate for electrochemical energy storage owing to their relatively long cycle life and high energy efficiency, their limited energy density as well as high cost are still causing a bottleneck for their long-term application. Alternatively, rechargeable Li-O_2 batteries have the potential to practically provide 3-5 times the gravimetric energy density of conventional Li-ion batteries. However, the lack of advanced electrode design and efficient electrocatalysts for oxygen reduction/evolution reactions remains as one of the grand challenges before this technology can be commercialized. Among various catalyst formulations, nanocarbon composite materials have been recognized as the most promising ones for Li-O_2 batteries because of its reasonable balance among catalytic activity, durability, and cost. In this perspective, the recent progress in the development of nanostructured carbon-based electrocatalysts for nonaqueous Li-O_2 batteries are discussed, including metal-free carbon catalysts, transition-metal-nitrogen-carbon composite catalysts, and transition metal/carbon compound catalysts. The morphology-performance correlations for these catalysts are discussed, aiming to provide rational guidance for designing advanced catalysts.

1. Introduction

The electrification of transportation and large-scale deployment of renewable energy have been the indispensable strategies for addressing the issues with global climate change, energy security, and sustainability. Lithium-oxygen (Li-O_2) batteries have been viewed as the most promising electrochemical energy storage technology to meet the transportation application in the near future, due to the highest theoretical energy density.[1-3] Unlike traditional Li-ion batteries, Li-O_2 batteries abandon the intercalation electrodes and Li^+ ions react directly with O_2 from the air in a porous electrode. As a result, the unique battery chemistry and electrode architecture provide a greatly increased specific energy density (theoretical value of 5200 Wh kg^{-1}).[2] Generally, Li-O_2 batteries can be divided into four different categories based on the electrolyte used in batteries: nonaqueous, aqueous, hybrid, and all-solid-state batteries. Currently, due to the insufficient ionic conductivity of solid-state electrolyte,[4] liquid electrolytes including nonaqueous and aqueous systems are extensively investigated. Their fundamental electrochemical reactions are compared in the following:

Anode: $Li \leftrightarrow Li^+ + e^-$ (1)

Nonaqueous cathode:

$2Li^+ + 2e^- + O_2 \leftrightarrow Li_2O_2$ ($E_0 = 2.96$ V *vs*. Li/ Li^+) (2)

Aqueous (Alkaline) cathode:

$O_2 + 2H_2O + 4e^- \leftrightarrow 4OH^-$ ($E_0 = 3.43$ V *vs*. Li/ Li^+) (3)

Aqueous (Acid) cathode:

$O_2 + 4e^- + 4H^+ \leftrightarrow 2H_2O$ ($E_0 = 4.26$ V *vs*. Li /Li^+) (4)

The use of a nonaqueous media in a Li-O_2 battery proved to be more feasible than aqueous electrolyte to alleviate parasitic corrosion on Li metal at the anode.[5,6,7] Furthermore, the theoretical energy density of a nonaqueous Li-O_2 battery is higher than that of an aqueous battery, because water or acid would be involved in the reactions in the aqueous system. Thus, to date, the nonaqueous configuration has attracted the most attention worldwide compared to other electrolyte-based Li-O_2 batteries.

Differing to aqueous systems where H_2O or H_2O_2 are produced during the oxygen reduction reaction (ORR) associated with discharging process, however, insoluble lithium-oxygen species (Li_2O_2) are formed in nonaqueous media and passivate the catalysts, eventually leading to a

termination of the discharge process. In addition, the intermediates in Li-O_2 electrochemical reactions, for example, O_2^-, O_2^{2-}, and LiO_2/LiO_2^-, are very reactive.[8-10] They can easily decompose most organic solvents. This leads to Li-O_2 battery discharge products of Li_2CO_3, LiOH, and lithium alkyl carbonates,[11,12] instead of only the desired product Li_2O_2 which can make a Li-O_2 battery truly rechargeable.[13,14] Thus, besides of cathode catalysts, exploring stable electrolyte still remains a grand challenge for rechargeable Li-O_2 batteries. During the charge process, the catalysts can be exposed again, corresponding to oxygen evolution reaction (OER), when an external potential is applied $E > E_0$, accompanied by the decomposition of these solid-state lithium-oxygen compounds. Thus, an efficient OER catalyst to catalyze a fast decomposition is needed to recover active sites for the ORR in next discharge-charge cycle. However, ORR and OER mechanisms in aqueous electrolyte are not effective in nonaqueous Li^+ electrolytes wherein various reactants/products and reaction intermediates are often insoluble. The catalyst properties required for efficiently catalyzing oxygen reactions in nonaqueous electrolytes are therefore different than those in aqueous media.

Like aqueous media, in nonaqueous Li^+-O_2 systems, a large ORR overpotential is also observed on currently used carbon cathode catalysts, causing significant losses in the battery discharge voltage (2.5 V) and low overall charge-discharge efficiency.[15] Specifically, the voltage gap between the charge and discharge of a Li-O_2 battery is larger than 1.0 V,[16] which results in a much lower voltage efficiency of <60%, relative to a Li ion battery (>90%). An additional challenge for the cathode catalysts for nonaqueous Li-O_2 batteries is that the catalysts should be designed to generate ORR products that can be efficiently decomposed during the subsequent OER for the rechargeable Li^+-O_2 system. Thus, the development of bifunctional ORR/OER catalysts with high activity and durability is desperately needed.

Early Li-O_2 experiments exhibited high overpotentials for the ORR and the OER during discharge (~0.5 V) and charge (~1.0 V) processes, respectively. These overpotentials result in large energy storage inefficiency. Simultaneously mitigating these ORR and OER overpotentials is a grand challenge to be overcome in the development of rechargeable Li-O_2 batteries. It was found that the ORR overpotential in nonaqueous electrolyte depends on the intrinsic activity of catalysts.[16,17] From the electrocatalysis point of view, catalysts play more significant role in the ORR than in the OER.[18] The discharge potentials were found greatly dependent on the cathode catalysts.[19,20] On the other hand, compared to pure carbon, no difference in catalytic activity for the OER is observed using the Au, Pt, or MnO_2 catalysts.[18] The OER during the charge process is greatly dependent on many non-catalysis related factors, such as the diffusion rate of the insoluble species (Li_2O_2), and electron transports rate on Li_2O_2.[21]

Hence, it is generally believed that electrocatalysts and the resulting electrode structures are critical to improving the power density, cycling capability, and round-trip energy efficiency of Li-O_2 batteries.[22,23] Especially, lowering the overpotential during discharge and charge is of prime importance in order to avoid carbon corrosion and to diminish electrolyte oxidation. The fundamental principles of electrocatalyst design for Li-O_2 nonaqueous system could be learned from aqueous oxygen electrochemistry, especially fuel cells and alkaline metal-air batteries. Carbon materials with more defects/functional groups and larger surface areas have exhibited better performance in nonaqueous Li-O_2 battery, similar to the case of ORR in aqueous solutions.[16,24] On the other hand, electrocatalysts for nonaqueous Li-O_2 batteries should promote the formation/decomposition of Li_2O_2 exclusively and suppress the formation of other lithium compounds (Li_2CO_3, LiOH, etc.), because only Li_2O_2 can be sustainably recharged.

Currently, catalysts based on such precious metals as Pt, Pd, Ir or Au represent the state of the art for oxygen reactions in both aqueous and nonaqueous electrolytes from the point of view of activity and durability.[1,25-29] Unfortunately, the prohibitive cost and scarcity of precious metals have limited their widespread implementation. Alternatively, non-precious metal catalysts (NPMCs) synthesized from earth-abundant elements (*e.g.,* Fe, Co, N, C) have the potential to efficiently catalyze these electrochemical reactions to realize the energy storage and conversion. The studied NPMCs include organometallic components, nonprecious-metal chalcogenides, and nitrogen-doped carbon catalysts.[25,30-33] In particular, recent breakthroughs in the development of high-performance NPMCs for the ORR and OER at Los Alamos National Laboratory (LANL)[19,20,24,27,33-42] and other research centers[24,43-53] show that carbon-based composite catalysts possess high activity and stability in both aqueous and nonaqueous electrolytes. Among various carbon-based catalyst formulations, nanostructured carbon materials with or without transition metals (*e.g.,* Co, Fe, Mn, Cu) have been recognized as the most promising ones for Li-O_2 batteries because of its reasonable balance among catalytic activity, durability, and cost.[3,54]

Especially, heteroatom (*e.g.,* N, S, B, or P) doping can tune the electronic and geometric properties of carbon, providing more active sites and enhancing the interaction between carbon structure and active sites. Importantly, involvement of transition metals (M) appear necessary for achieving high catalytic activity and improved durability of heat-treated NPMCs by catalyzing carbonization of nitrogen/carbon precursors to form highly graphitized carbon nanostructures (*e.g.*, tubes, onion-like carbon, multi-layered graphene) with more favorable nitrogen doping.[19,36,38,55] However, the exact nature of the active sites in the metal-nitrogen-carbon (M-N-C) catalyst remains the subject of intense debate in the field. It is unknown whether the transition metals participate in the active sites or simply catalyze their formation. In either case, the nitrogen species embedded within the carbon structures are likely critical to the active-site performance. Most recently, a new class of nanocarbon/ metal oxides or sulfides hybrid catalysts for the ORR in alkaline media was emerged. With such unique configurations, a synergetic effect may rise between the active species in nanocarbon and these loaded oxides/sulfides, resulting in much improved activity.

In this perspective, the recent efforts in the development of nanostructured carbon-based electrocatalysts for nonaqueous Li-O_2 batteries are highlighted, with special focus on ORR catalysts. Catalyst materials discussed include metal-free carbon catalysts, nanostructured transition-metal-nitrogen-carbon composite catalysts and transition metal/carbon compound catalysts.

2. Nanocarbon cathode catalysts

2.1 Metal-free carbon catalysts

Recently, the research on exploring the use of carbon nanocomposites as metal-free cathode catalysts has been one of the major subjects for Li-O_2 batteries. Due to the low cost, large

surface area, corrosion resistance, high electrical conductivity, and good ORR/OER activity, carbon materials are viewed as ideal candidates for metal-free cathode in Li-O_2 batteries. A carbon-based air electrode was first studied in a nonaqueous Li-O_2 battery by Abraham and coworkers.[56] Based on a polymer electrolyte and a 0.3 mm thick air electrode, a specific capacity of 1600 mAh g^{-1} carbon was obtained. It was found that the specific capacity of Li-O_2 batteries decreases with decreasing surface area of the carbon cathode. The performance of Li-O_2 batteries is influenced by several other factors, including carbon types,[57] carbon loading,[56] oxygen partial pressure,[58] and electrolyte selection.[58-60] These factors are directly related to the oxygen diffusion process in the air electrode. On the other hand, the ORR associated with the discharging process at the air electrode primarily produces insoluble Li_2O_2 particles in a nonaqueous Li-O_2 cell, which accumulates at the active sites of the air electrode, potentially clogging the pores and thus increasing the resistance of gas transport through the pores. In addition, the catalytic activity of the electrode will also be deactivated by the poor conductivity of the insulating Li_2O_2.[61] Therefore, the structure of carbon used in the air electrode is a critical factor that affects the performance of Li-O_2 batteries.

Several works have reported that the specific energy of Li-O_2 batteries increased with increasing mesopore volume of carbon catalysts used in their air electrodes.[57,62] The reasons, which the real capacity of a Li-O_2 battery does not correspond to the theoretical capacity of metallic lithium, result from the insolubility of discharge products (Li_2O_2 and Li_2O) in nonaqueous organic electrolytes.[63] Instead, the real capacity that a Li-O_2 battery can achieve is determined by the carbon-based air electrode, especially with respect to the pore volume available for the deposition of discharge products, rather than the lithium anode. Different commercial carbon materials, such as BP2000 (Cabot Corp.), Calgon (Calgon Carbon Corp.), Denka (Denka Corp., Japan), Ketjenblack (KB) (Akzo Nobel Corp.), and Ballmilled KB were investigated for their applications in air electrodes of Li- O_2 batteries,[57] which the effects of pore size distribution and pore volume in different carbon sources were determined. Among the studied carbon materials, KB has both relatively uniform pore size (3-10 nm) and high pore volume, whereas the other commercial carbon materials show less uniform pore size and low pore volume. In the Li-O_2 battery test, KB, which has the highest mesopore volume among all of the carbon sources tested in this work, demonstrated the highest specific capacity when operated in a dry air environment where the oxygen partial pressure is 0.21 atm. After soaking in the electrolyte, the KB-based electrode expanded significantly (>100%) and absorbed much more electrolyte than electrodes made of other types of carbons. The large volume expansion in the KB-based electrode led to extra triphase regions to facilitate the Li-O_2 reaction in the electrode and extra volume to accommodate the reaction product (Li_2O/Li_2O_2). Consequently, the Li-O_2 cells using KB-based air electrode exhibited the highest specific capacity among all samples. With optimized electrode porosity/thickness and electrolyte amount, a high capacity of 1756 mAh $g_{\text{-carbon}}^{-1}$ corresponding to an area-specific capacity of 26.5 mAh cm^{-2} was obtained for a Li-air battery operated in a dry air environment.

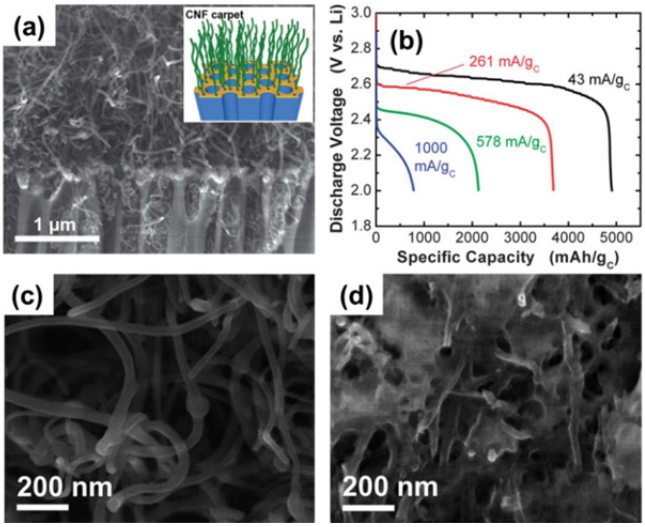

Fig. 1. (a) Cross-sectional SEM image of the AAO filter after nanofiber growth. Inset: schematic representation of the electrode after catalyzed growth of carbon nanofibers. (b) First-discharge rate capability of CNF electrodes with galvanostatic currents corresponding to 43, 261, 578, and 1000 mA g_{cat}^{-1}. (c) SEM image of CNF electrode after discharge to a capacity of 350 mAh g_{cat}^{-1} at 68 mA g_{cat}^{-1}. (d) SEM image of CNF electrode after full discharge to a capacity of 7200 mAh g_{cat}^{-1} at 63 mA g_{cat}^{-1}. Reproduced with permission from Ref. 15 Copyright (2011) Royal Society of Chemistry.

Recently, a new approach to fabricating porous carbon air electrode was demonstrated by Shao-Horn's group.[15] Vertically aligned arrays of hollow carbon nanofibers (CNFs) with diameters on the order of 30 nm were fabricated using atmospheric pressure chemical vapor deposition (CVD) on porous anodized aluminium oxide (AAO) substrates coated with thin layers of Ta and Fe (**Figure 1a**). The Li-O_2 cells based on the CNFs air electrode discharged at an average voltage of 2.61 V over the entire discharging process and achieved a gravimetric discharge capacity of 4720 mAh g_{cat}^{-1} at low rates (**Figure 1b**). The gravimetric energy densities was measured up to ~2500 Wh $kg_{discharged}^{-1}$ at power densities up to ~100 W $kg_{discharged}^{-1}$, which translated to an 4-times energy enhancement that for the state-of-the-art lithium intercalation compounds such as $LiCoO_2$ (~600 Wh kg^{-1}). The good electrochemical performance was attributed to the more porous structure than other carbon materials, which enhanced utilization efficiency of the available carbon mass and void space for Li_2O_2 deposition during discharge. Additionally, the electrodes demonstrated reasonable reversibility over the first 10 cycles at a moderate rate (300 mA g_{cat}^{-1}). The observations of Li_2O_2 formation and morphological evolution during discharge were also conducted. Cross-sectional ex-situ SEM imaging of the electrode revealed that Li_2O_2 appeared to first form as discrete spherical particles on the CNF sidewalls. Li_2O_2 structures were found to evolve from spherical particles, with an average diameter of ~100 nm at 350 mA h g_{cat}^{-1} (**Figure 1c**), to toroidal-shaped particles, with an average diameter of ~400 nm at 1880 mAh g_{cat}^{-1}. These particles were observed to grow as large as ~1 μm diameter with increasing depth-of-discharge, before eventually merging into a monolithic mass (**Figure 1d**).

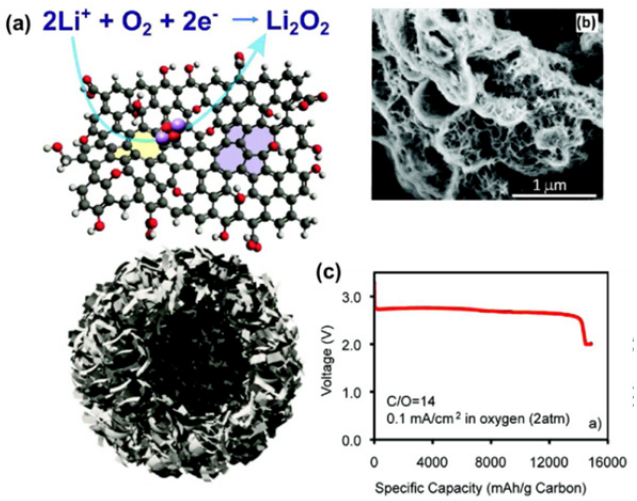

Fig. 2. (a) Schematic structure of a functionalized graphene sheet (upper image) with an ideal bimodal porous structure (lower image) which is highly desirable for Li-O_2 battery operation. (b) SEM images of as-prepared FGS (C/O = 14). (c) The discharge curve of a Li-O_2 cell using FGS(C/O =14) as the air electrode (P_{O2} = 2 atm). Reprinted with permission from ref. 24 Copyright (2011) American Chemical Society.

Generally, among different allotropes of carbon, carbon materials with ordered graphitic structure are expected to facilitate the electron transfer rate and exhibit good electrochemical stability. Particularly, graphene, a one-atom thick sheet of sp^2-bonded carbon, is of particular interest in developing advanced energy materials due to its unique physical and chemical properties, such as high surface area (theoretical value: ~2630 $m^2 g^{-1}$), high chemical stability, excellent conductivity, unique graphitic basal plane structure, and the easiness of functionalization.[64,65] Importantly, graphene nanosheets (GNSs) have been successfully established in air electrode for both nonaqueous[66,67] and hybrid electrolyte[68] Li-O_2 batteries. In a nonaqueous Li-air battery, the air electrode based on GNSs yielded a high discharge capacity of ~8700 mAh g^{-1} at a current density of 75 mA g^{-1}, compared to ~1900 mAh g^{-1} for BP-2000 and ~1050 mAh g^{-1} for Vulcan XC-72, respectively. The dominant discharge product was Li_2CO_3 and a small amount of Li_2O_2. This result indicated that GNSs can be used as an ideal candidate for Li-air batteries. Recently, Xiao and coworkers used a colloidal microemulsion approach and demonstrated the construction of hierarchically porous air electrodes with functionalized graphene sheets (FGSs) that contain lattice defects and hydroxyl, epoxy, and carboxyl groups. **Figure 2a** shows the schematic structure of functionalized graphene with an ideal bimodal porous structure which is highly desirable for Li-O_2 battery operation. Unlike conventional two-dimensional (2D) layered graphene sheets that hinder the rapid gas diffusion that is essential for the efficient operation of Li-air batteries, the three-dimensional (3D) air electrodes developed in this work *via* the thermal expansion and simultaneous reduction of graphite oxide consist of interconnected pore channels on both the micro- and nanometer length scales (**Figure 2b**), is ideally suited for air electrodes since the pores on different length scale may facilitate oxygen diffusion, avoiding pore blockage due to Li_2O_2 deposition during discharge in nonaqueous Li-O_2 batteries. Density functional theory (DFT) calculation and electron microscopy characterization suggest that the functional groups and lattice defects play a critical role in improving the battery performance by forming small particle size of discharge products. In particular, the C/O = 14 graphene electrode, containing more functional groups, resulting in better performance and smaller Li_2O_2 particles, when compared to those of C/O = 100 with less functional groups. Importantly, in the unique hierarchical structures, large tunnels constructed by the macro-pores facilitate oxygen transfer into the air electrode, and small "pores" is able to provide ideal multi-phase regions for the ORR. Thus, the combination of the abundance of functional groups and the hierarchical pore structures leads to an exceptionally high capacity of 15000 mAh g^{-1} during the discharge process (**Figure 2c**).

Apart from pristine carbon materials, it is well known that chemical doping with heteroatoms (*e.g.*, N, B, P, or S) into carbon lattice can tune the electronic and geometric properties,[69] thereby providing more active sites, and enhancing the interactions between carbon structure and oxygen molecules toward the ORR in aqueous solution. Among various heteroatoms, nitrogen doping plays a critical role in modifying carbon materials due to comparable atomic size of nitrogen and carbon, as well as the presence of five valence electrons in the nitrogen atoms available to form strong covalent bonds with carbon atoms. It was experimentally proved that the nitrogen-doped carbon materials turn out to be more compartmentalized and disordered than undoped analogues.[70] Those defects may serve as active sites and result in much stronger adsorption of oxygen molecule. These experimental observations are in good agreement with theoretical studies that nitrogen can be viewed as an *n*-type carbon dopant, donating electrons to carbon, and facilitating the ORR.[71] Various nitrogen doping into carbon *via* heat treatment at high temperatures (800°C-1000°C) can be identified by different XPS binding energies associated with pyridinic (398.6 ± 0.3 eV) and graphitic nitrogen (401.3 ± 0.3 eV).[69] Specifically, pyridinic nitrogen is obtained by doping at the edge of the graphene layer, contributing one p_π electron to the graphitic π system. Graphitic nitrogen is the result of in-plane doping and contributes two p_π electrons. Recently, it was reported that nitrogen-doped carbon nanotubes (N-CNTs) exhibited a specific discharge capacity of 866 mAh g^{-1} in a nonaqueous Li-O_2 battery, which was about 1.5 times higher than pristine CNTs (590 mAh g^{-1}).[72] This example demonstrates that, like in aqueous solution, nitrogen doping to carbon materials is also able to efficiently enhance the ORR activity in nonaqueous electrolyte.

Later, the nitrogen-doped graphene nanosheets (N-GNSs) as cathode materials exhibit excellent electrocatalytic activity for Li-O_2 batteries.[73] From rotating disk electrode (RDE) measurements, the N-GNSs prepared by post heating the GNSs under high purity ammonia mixed with Ar at 900°C for 5 min exhibited positively shifted onset potential of ORR relative to that of GNSs in O_2-saturated 0.1 M $LiPF_6$ in tetraethylene glycol dimethyl ether (TEGDME) solution (**Figure 3a**). Noteworthy, there is no well-defined diffusion limiting current plateau for both samples, probably due to the coverage of active sites by *in-situ* formed insoluble Li_2O_2 thereby making the ORR in nonaqueous electrolyte kinetically sluggish. Furthermore, the numbers of electron transferred in the ORR estimated from Tafel-slops are 0.99 for N-GNSs and 0.80 for GNSs, respectively, suggesting that N-GNSs have higher catalytic activity in a nonaqueous solution. In Li-O_2 battery testing, the initial discharge capacity of GNSs electrode is 8530 mAh g^{-1} at a current density of 75 mA g^{-1}, while 11,660 mAh g^{-}

[1] was measured with the N-GNSs, about 40% higher than that of GNSs (**Figure 3b**). The morphologies of discharge products (discharged for 1 h) for GNSs and N-GNSs electrodes are shown in **Figure 3c** and **3d**, respectively. It can be seen that the morphologies of the products on the two surfaces are significantly different. On GNSs, the product particle size is distributed from 20 to 45 nm, whereas on N-GNSs, a smaller size from 5 to 20 nm was observed. Moreover, the distribution of the product is more uniform on N-GNSs, while the product particles aggregated into large clusters on GNSs and some surfaces are free of coverage. These observations suggest that the presence of the homogeneously distributed nitrogen species resulting in more active sites (defects and functional groups) of N-GNSs provides more nucleation sites and thus promotes a more uniform dispersion of discharging products.

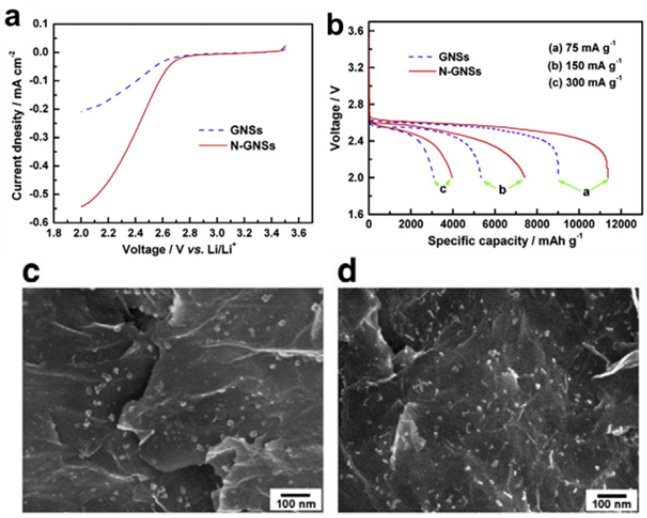

Fig. 3. (a) rotating-disk electrode voltamograms recorded for GNSs and N-GNSs electrodes for ORR at a rotating speed of 100 rpm in O_2-saturated 0.1 M $LiPF_6$ in TEGDME solution at a scan rate of 5 mV s^{-1}. (b) Discharge profiles of GNSs and N-GNSs electrodes at various current densities. (c, d) SEM images of the GNSs (c) and N-GNSs (d) electrodes discharged for 1 h. Reprinted with permission from ref. [73] Copyright (2012) Elsevier.

2.2 Nanostructured Metal-Nitrogen-Carbon Catalysts

2.2.1 Catalyst synthesis strategies

Although catalysts with respectable ORR activity can be prepared without any detectable metal content,[43,46,74] so far the presence of Fe and/or Co can yield catalysts with much enhance activity and better durability compared to metal-free catalysts.[25,31] This is most likely due to either promotional role of transition metal to accelerate nitrogen doping into carbon matrix, or directly participate into active site constitution with improved intrinsic activity toward the ORR.[75] Pioneered by Jasinski [76] and Yeager [77] who developed the metal-nitrogen-carbon (M-N-C, M: Co/Fe)) type of NPMCs by pyrolyzing transition-metal macrocycles at temperatures exceeding 700°C for the first time and demonstrated significantly enhanced ORR activity and stability of the resulting catalysts relative to the performance of un-heated macrocycles. In an effort to explore this kind of pyrolyzed catalysts, different catalysts have been prepared in a similar manner, using a wide variety of N-containing chemicals as the starting materials, many of which are no longer macrocyclic. Because these metallo-porphyrins and metallo-phthalocyanines are considered to be extremely hard to synthesize due to a number of steps required, resulting in high manufacturing prices and outweighing the benefit of the low initial materials cost. To date, the M-N-C types of non-precious metal catalysts (NPMC) have been widely recognized as the-state-of-the-art catalyst formulation toward ORR in both acid[34,78] and alkaline[79] electrolytes. Much enhanced stability (700 hours at 0.4V)[34] and volumetric activity (230 A cm^{-3})[80] of M-N-C catalysts have been demonstrated in low-temperature proton exchange membrane (PEM) fuel cell operations.

In general, the formation mechanism of active site on such-fabricated catalysts has not been unambiguously determined. Dodelet *et al*. has indicated that the ORR active site in M-N-C catalysts involves MN_x/C-type species (M: Co and Fe).[78] Later, the possible Fe-N_x coordination in polyaniline (PANI)-Fe-C catalysts through high-temperature treatments has been verified by X-ray absorption near-edge structure (XANES) and extended X-ray absorption fine structure (EXAFS) spectroscopies, which enable the measurement of atomic structure, bonding characteristics, and oxidation state with elemental specificity in the catalysts.[24,81,82] Such Fe-N_x coordinations (*e.g.,* pyridinic Fe-N_{2+2+2}, pyrrolic Fe-N_4, and porphyrazin Fe-N_4) are able to be survived after heat treatments and has been clearly correlated with the ORR activity.[81] Although it is generally accepted that heat-treatment steps are indispensable to activity and stability improvements, the enhanced performance of the catalysts remains strongly dependent on the synthetic methods including carbon support used, source of metal and nitrogen, thermal treatment conditions, and supporting templates.[27] The type of transition metals in the precursors has been proven to play a critical role in the M-N-C catalysts and can be tied to activity enhancement after the heat treatment.[83,84] In one type of catalyst derived from polyacrylonitrile, metal, and carbon, Fe and Co lead to the formation of the active centers with higher activity towards the ORR in alkaline solution, when compared to other transition metals (*e.g.,* Zn, Ni, Mn, Cu, Cr).[83] Nitrogen precursors used in the synthesis were found to be of great significance to the ORR activity and durability. Generally, three different groups of nitrogen precursors have been employed to develop M-N-C catalysts in alkaline media: (1) C≡N-based non-aromatic precursors, like cyanamide[79,85] and dicyanamide;[86] (2) C-N-based non-aromatic amine precursors, like ethylenediamine (EDA);[87] (3) aromatic precursors, like aniline and melamine.[34,88]

Like in aqueous electrolyte, such-synthesized M-N-C catalysts also exhibit high catalytic activity for the ORR in the nonaqueous solution for Li-O_2 battery cathodes.[16,54] The catalytic performance of an M-N-C composite was evaluated for the first time in connection with rechargeable Li-O_2 battery application by Liu and coworkers. The studied Fe-N-C catalysts were synthesized *via* the pyrolysis of iron acetate, 1,10-phenanthroline, and carbon black (Black Pearls 2000) at 1050°C for 0.3 h, following by acid leaching and second heat-treatment which are typical approaches for developing such kind of M-N-C catalysts (**Figure 4a**).[51] In particular, the majority of the Fe centers in these samples were present in non-square planar configurations through an axial ligation as verified by X-ray absorption spectroscopic techniques, which was consistent with an average ligation number higher than 4 derived from the EXAFS analysis. In the Li-O_2 battery tests, the developed catalyst produced lower charge-discharge

overpotentials, when compared to the well-studied α-MnO_2/XC-72 (**Figure 4b**) and carbon only counterparts. Effluent gas analysis by gas chromatography (GC) at the end of controlled discharge-charge cycles demonstrated no CO_2 formation for cathode made of the Fe-N-C catalyst (**Figure 4c**), suggesting it selectively promoted the decomposition of Li_2O_2, rather than the electrolyte. In the contrast, both α-MnO_2/XC-72 and carbon black revealed significant CO_2 production during the charging process, indicative of electrolyte decomposition. Such improved selectivity led to an enhanced battery lifespan under controlled cycling, with 50 discharge-charge cycles achieved as shown in **Figure 4d**. Such improved cyclability measured in M-N-C can be primarily attributed to the highly graphitized carbon structures formed in high-temperature treatments, which are strongly tolerant to carbon corrosion, especially at high potentials. This pioneering study demonstrates that the M-N-C types of catalysts derived from earth-abundant elements could not only activate the ORR but also promote the OER, holding great promise as efficient bifunctional electrocatalysts for rechargeable nonaqueous Li-O_2 battery application.

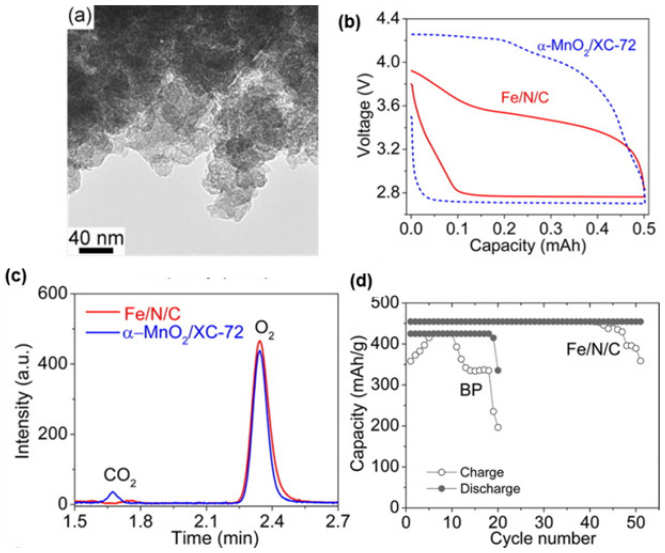

Fig. 4. (a) TEM image of the developed Fe-N-C catalysts. (b) Discharge/charge voltage profiles of Li-O_2 cells using α-MnO_2/XC-72 and Fe/N/C as cathode catalysts. (c) Representative GC signals as a function of retention time for the gas effluents collected at the end of the charging processes. (d) Cycling performance of cells with catalysts Fe/N/C and carbon black (BP) as cathode catalysts, current was 0.05 mA with duration of 5 h. Reprinted with permission from ref. [51]. Copyright (2012) American Chemical Society.

2.2.2 Promotional role of graphene morphology

In our recent effort in developing carbon-based ORR M-N-C catalysts (M: Fe or Co), in situ formation of various carbon nanostructures with nitrogen doping can be realized by catalyzing the decomposition of the nitrogen/carbon precursor at high temperatures (800-1000°C),[33,36] exhibiting high activity for the ORR. Importantly, we can control the formation of different nanostructures (*e.g.*, carbon nanotube, onion-like carbon, graphene) during the catalyst synthesis through optimizing the transition metals, nitrogen/carbon precursors, and templates.[33,36] Apart from the obvious advantages of high electronic conductivity and enhanced corrosion resistance, these highly graphitized carbon nanostructures present in the M-N-C may serve as a matrix for hosting nitrogen and metal moieties.[25] As shown in our previous nonprecious metal catalyst research, the presence of graphitized carbon appears to enhance stability of the ORR catalysts.[36] Targeting the application in nonaqueous Li-O_2 battery cathodes, a nitrogen-doped graphene-sheet-rich Co-N-C catalyst derived from PANI, cobalt, and multi-walled carbon nanotubes (MWNTs) was developed.[19]

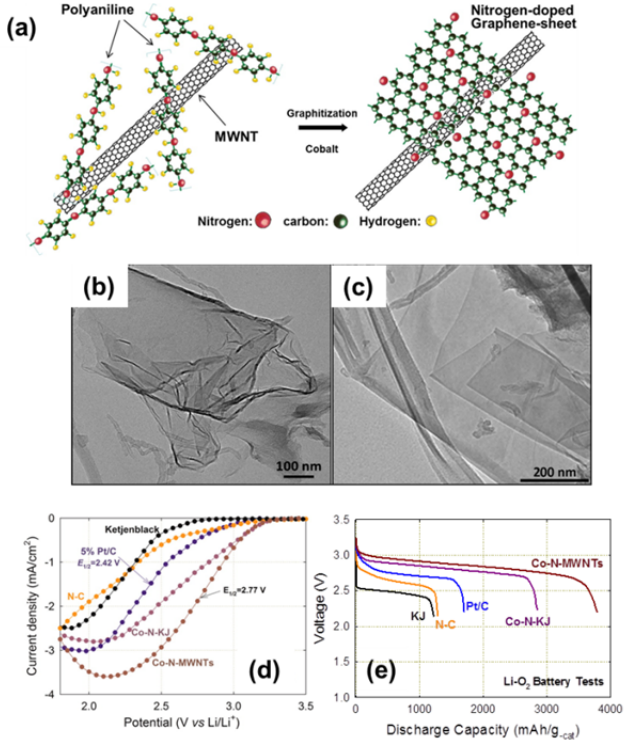

Fig. 5. (a) Scheme of the formation for nitrogen-doped graphene sheets derived from polyaniline and Co precursors using MWNTs as a template. (b, c) HR-TEM images of the graphene-rich nanocomposites observed in Co-N-MWNT catalysts. (d) RDE testing results for the ORR at 25°C in oxygen-saturated 0.1 M $LiPF_6$ in 1,2-dimethoxyethane electrolyte at a rotating speed of 900 rpm on various catalyst samples. (e) Initial discharge performance for various catalysts at a current density of 50 mA g_{cat}^{-1} in Li-O_2 battery tests. Reprinted with permission from ref. 19. Copyright (2012) American Chemical Society.

A synthesis scheme for the nitrogen-doped graphene composites is shown in **Figure 5a**.[19] As a both nitrogen and carbon source, the heteroatom polymer, PANI, was graphitized at elevated temperature with the catalysis of a Co species. Due to their structural similarities, the aromatic in PANI may facilitate the graphitization process and form nitrogen-doped graphene-sheet-like structures (**Figure 5b** and **5c**).[19] In the RDE test (**Figure 5d**),[19] as discussed above, no saturated plateau at low potential range is achieved for ORR in the nonaqueous electrolyte.[89] Instead, a broad peak was observed at the low potential range. This is due to the formation of insoluble lithium-oxygen compounds that cover the catalyst surface, ultimately resulting in a degradation of catalyst activity. It is worth noting that the resulting Co-based catalysts

exhibit superior performance compared to Pt catalysts and other controls, reflected by a positive difference in the ORR half-wave potential, $E_{1/2}$ (2.42 V for Pt *vs*. 2.77 V for Co-N-MWNTs) and, to a lesser degree, by a difference in the onset potential (3.0 V for Pt *vs*. 3.1 V for Co-N-MWNTs). In nonaqueous Li-O_2 battery tests, the Co-N-MWNT catalysts also deliver the highest initial discharge capacity (~3700 mAh g_{cat}^{-1}) among the studied catalysts (**Figure 5e**). Furthermore, the cell showed very good cycling stability up to 20 cycles without significant capacity loss; further cycling to 30 and 50 cycles results in capacity losses of 8.4 and 20.4%, respectively. MWNTs proved to be an effective supporting template for the formation of graphene, as compared to traditional carbon black supports. As the MWNTs still obviously present in the catalysts after heating treatment, the graphene-like sheets are likely not derived from the carbon nanotubes. Importantly, optimized heating temperatures lead to a maximum in the yield of graphene structures in the final catalyst. The graphene-sheet-like structures grown over the solid particles are only observed when the heat-treatment temperature reaches 900°C, which are in good agreement with the highest BET surface areas (278 m^2 g^{-1}) and maximum ORR activity in nonaqueous electrolyte measured with the samples synthesized at 900°C. On the other hand, properly selecting the transition metal in synthesis is also a key to controlling the graphene morphology and doped nitrogen structure.

2.2.3 Role of transition metals

Here, when PANI was used as nitrogen-carbon precursors, the effect of transition metals used during the synthesis on ORR activity in both aqueous and nonaqueous was discussed. Although these results are not universally valid for other nitrogen-carbon precursor-derived catalysts, the finding may provide some insights into the optimal active sites for the ORR in nonaqueous electrolyte.

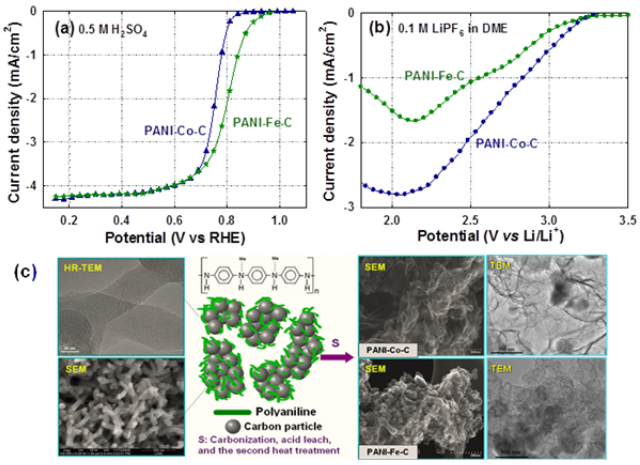

Fig. 6. Catalytic activity for the ORR in (a) aqueous and (b) nonaqueous electrolytes, and (c) catalyst morphologies and structures for PANI-Fe-C and PANI-Co-C catalysts. Reprinted from ref. 41 with permission of The Royal Society of Chemistry. Reprinted with permission from ref. 19. Copyright (2012) American Chemical Society.

As shown in **Figure 6a** and **6b**, the PANI-Fe-C catalysts usually exhibit higher activity for ORR in traditional aqueous electrolyte; however, in nonaqueous Li electrolyte, the PANI-Co-C catalysts show better activity for the ORR.[19,41] These results suggest that the optimal active site structures for the ORR in both aqueous and nonaqueous media are different. It will be very interesting to further understand why these two kinds of catalysts perform so differently in aqueous and nonaqueous electrolytes. At first, in order to determine the role of Co and Fe in catalyst synthesis, especially during the graphitization of PANI, nanostructure and morphology of PANI-Fe-C and PANI-Co-C catalysts were compared using electron microscopy (**Figure 6c**). It was found that graphene-sheet structures abundantly exist in the PANI-Co-C catalyst, but not in the PANI-Fe-C catalyst. This significant difference in catalyst nanostructures implies that Co probably is more effective to catalyze PANI decomposition to the atomic level, and then these carbon and nitrogen atoms re-arrange and coalesce together, forming highly graphitic N-doped graphene structures.

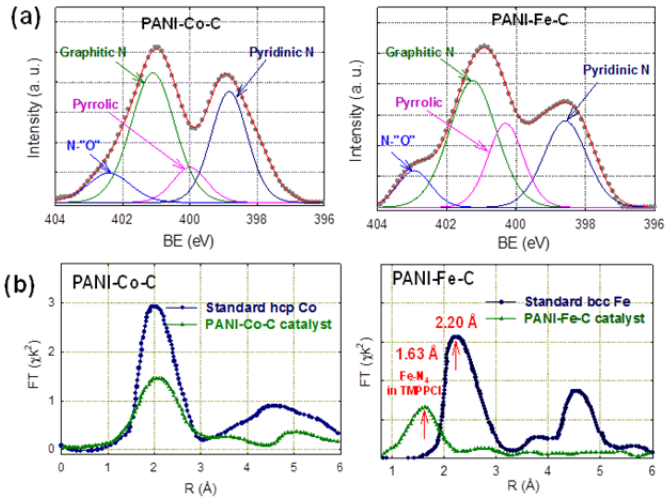

Fig. 7. XPS (a) and XAS (b) for PANI-Fe-C and PANI-Co-C catalysts. Reprinted with permission from ref. 41 Copyright (2011) Royal Society of Chemistry.

In the meantime, as the nitrogen functional structures had been believed to be important for active sites, the effect of transition metals on nitrogen doping was further studied using XPS (**Figure 7a**). It was found that the addition of Co leads to a relatively higher pyridinic nitrogen, capable of catalyzing nitrogen doping at the edge of graphene planes. On the other hand, Fe may play a promotional role to increase graphitic nitrogen and catalyze nitrogen doping at the center of graphene. In order to get more detailed bonding structure information for these transition metals in catalysts, ex-situ X-ray absorption was used to analyze these PANI-Fe-C and PANI-Co-C catalysts (**Figure 7b**). In the case of PANI-Co-C catalysts, similar to standard cobalt metal (hcp), dominant peak in PANI-derived Co catalyst is around 2 Å, belonging to Co-Co shell. This result indicates that the principal Co species in catalyst is highly metallic and no Co-N coordination was found. Importantly, similar results had been found in another Co catalyst derived from EDA, a different nitrogen-carbon precursor.[44] When pyrolysis temperature is above 800°C, Co-N bonds formed in the room temperature were completely broken and metallic Co-Co bonds newly formed.[44] In the case of PANI-Fe-C catalysts, the spectroscopy shows a dominant peak around 1.63 Å that is very close to a typical Fe-N_4 structures found in macrocyclic compounds. Thus, the Fe-N_x coordination structures are very

possible in the PANI-Fe-C catalyst. At this point, as Co-based catalyst has higher activity for the ORR in nonaqueous media, the metal-free pyridinic N dominant in PANI-Co-C catalysts seem to be important to ORR in nonaqueous media. However, the possible Fe-N_x coordination structures in PANI-Fe-C catalyst may directly participate into the active sites with higher intrinsic activity for the ORR in the traditional aqueous, compared to the metal-free nitrogen-doped carbon structures.

2.2.4 Unique templating role of MOFs

Another example demonstrating M-N-C catalysts for Li-O_2 battery cathode is graphene/graphene tube nanocomposites derived from dicyanamide, iron, and cage-containing metal-organic frameworks (MOFs).[20] MOF is expected to offer unique opportunities in synthesizing efficient ORR catalysts due to the accessibility of metal-cation centers, the variety of building blocks, and the high micropore surface area.[90] However, most studied MOFs as precursors for ORR catalyst synthesis are limited to commercially available microporous ones.

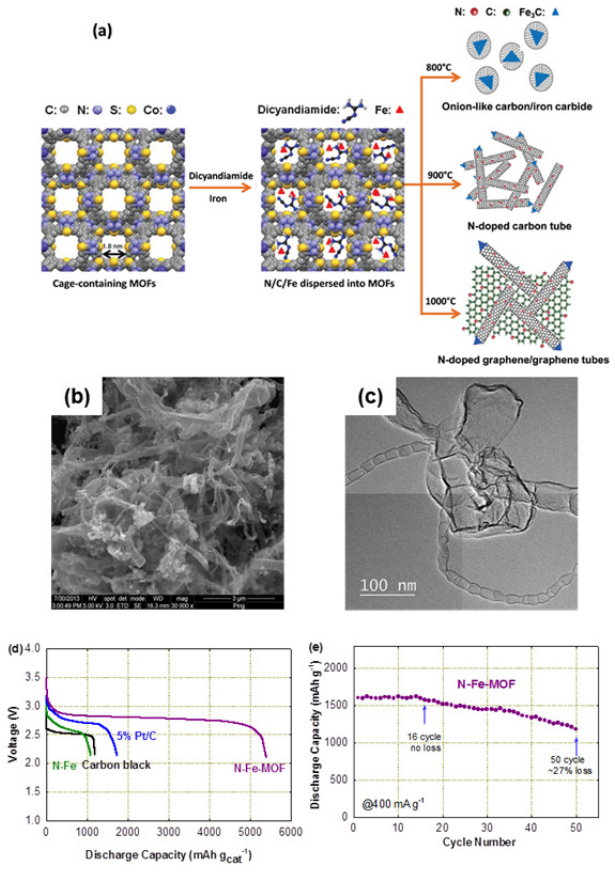

Fig. 8. (a) Schematic illustration of the formation of N-Fe-MOF nanostructures at different heating temperatures. (b, c) SEM and TEM images of N-Fe-MOF catalyst heat-treated at 1000°C. (d) initial discharge performance for various catalysts at a current density of 50 mA g_{cat}^{-1} in Li-O_2 battery tests, (e) cycling test of N-Fe-MOF catalyst at a current density of 400 mA g_{cat}^{-1} with voltage cutoff at 2.5 V (discharge) and 4.1 V (charge). Reprinted with permission from ref. 20. Copyright 2014 WILEY-VCH.

In that work, a newly-developed Co containing MOF material with giant polyhedral cages (cage size ~1.8 nm) was employed as a template in preparation of M-N-C ORR catalysts for nonaqueous Li-O_2 battery cathodes. Such MOF materials with large pores may be beneficial for synthesizing efficient ORR catalysts by well dispersing nitrogen/carbon precursors (dicyanamide), thereby significantly increasing the active-site density. The synthesis procedures of the MOF templating nitrogen-iron catalysts (N-Fe-MOF) are schematically illustrated in **Figure 8a**. Importantly, graphene/graphene tube structures can be only catalytically prepared by *in-situ* formed Fe_3C at heating temperature of 1000°C (**Figure 8b** and **8c**).

Other temperatures result in onion-like Fe/Fe_3C species (800°C and 1100°C) or only N-doped carbon nanotubes (900°C). Interestingly, the total nitrogen content for the N-Fe-MOF sample consistently decreases from 4.07 at.% to 2.07 at.% with increasing heating temperature from 800°C to 1100°C, without leading to a commensurate drop in ORR activity. The relative amount of graphitic nitrogen goes up as the heating temperature is increased, along with a commensurate enhancement in ORR activity, reaching maximum at 1000°C. Notably, an extremely high temperature (1100°C) results in significant reduction in pyridinic nitrogen on the prepared catalysts and is accompanied with a drop in ORR activity. The doped nitrogen atoms at the edge of the graphitic layers (pyridinic) are generally believed to be connected with ORR activity.[36,39] Importantly, the newly presenting results indicate that graphitic nitrogen and the optimal C-N_x configuration reflected by the ratio of the two of nitrogen functionalities may be as important as the pyridinic nitrogen toward the ORR activity enhancement in nonaqueous electrolyte. Due to the use of cage-containing MOF, the well-distributed nitrogen species into graphene/graphene tube nanocomposite was obtained from the optimized synthesis conditions, providing increased disorders and defects as nucleation sites for discharge products. As a result, in Li-O_2 battery tests, the N-Fe-MOF catalysts also deliver the highest initial discharge capacity (~5300 mAh g_{cat}^{-1}) among all the cathodes studied in that work (**Figure 8d**). In the meantime, the catalyst also exhibits enhanced OER activity and recharging capability in Li-O_2 battery tests. The cell revealed good cycling stability up to 16 cycles without significant capacity loss; further cycling to 50 cycles results in capacity losses of about 27% (**Figure 8e**). In fact, the cyclic durability of Li-O_2 batteries is one of the grand technical obstacles to commercialization of the advanced battery technology.[91] The accumulated insoluble solid particles remained in the charged products may block the catalyst sites and O_2 transfer channels in the electrodes, thereby leading to the observed degradation. In addition, the gradual loss of electrolyte due to possible evaporation is likely another reason for the observed performance degradation.

2.3 Carbon composites with metal oxides/nitrides catalysts

Apart from the nitrogen-doped carbon composite catalysts discussed above, transition-metal oxides (TMOs), transition-metal nitrides (TMNs) and mixed transition-metal oxides (MTMOs) with stoichiometric and even non-stoichiometric compositions have attracted increasing interests for the applications in nonaqueous Li-O_2 batteries.[3,49,54,81,92-99] TMOs, TMNs and MTMOs have several advantages such as low cost, controllable synthesis, tunable nanostructure, and relatively high ORR/OER activity. Importantly, unlike carbon-based catalysts prone to corrosion in nonaqueous Li-O_2 batteries,[100,101] TMOs, TMNs and MTMOs are stable over the operating

voltage of the cathode (typically 2-4 V *vs*. Li^+/Li) and able to bear the nucleophilic attack by O_2^- and O_2^{2-}. However, one of major drawbacks of TMOs, TMNs and MTMOs stems from their heavy molecular weight and low electrical conductivity, which likely lead to low energy density and power density of batteries. To address the problems caused by these unfavorable properties, conductive substrates are usually incorporated into the composites of TMOs, TMNs or MTMOs to improve the conductivity and utilize their catalytic activity to the greatest extent possible.[102] For example, a variety of carbon supports, such as porous carbon, carbon nanotubes, and reduced graphene oxide, have been used to improve electrical conductivity of TMOs or MTMOs and consequently enhance the capacity and cycling stability of Li-O_2 batteries.[37,103,104]

2.3.1 Mono metal oxide catalysts

Among different TMOs, MnO_x with different chemical composition and physical nanostructure is the most extensively studied catalyst in nonaqueous Li-O_2 batteries.[37,86,103,105-109] The surface properties of MnO_x related to electronic structure of active centers and the concentration level of the defects and vacancies play a critical role in the oxygen-involved electrochemical reaction in both aqueous and nonaqueous electrolyte.[94,110-112] The intrinsic catalytic activity of MnO_x in Li-O_2 batteries is dominated by electronic structures of active centers, on which the oxygen molecule is absorbed in the first step of ORR and then is reduced to superoxide radical ion in aprotic electrolyte.[93] The vacancy and defect on the surface of MnO_x catalysts greatly affect the electronic structure of manganese ion center and consequently change the binding energy of the oxygen molecules on catalyst surface. Like other oxides, the major disadvantage of MnO_x as a cathode catalyst in a Li-O_2 battery suffers from its inherently low electrical conductivity, yielding a high overpotential for ORR/OER in the nonaqueous electrolyte To effectively promote its catalytic activity in Li-O_2 batteries, many researchers tried to use conductive carbon materials incorporated with MnO_x to form composites, which are able to greatly enhance the electrical conductivity, and thus the battery performance.[37,105] In addition, the combination between TMOs and carbon substrate could also significantly affect the catalytic activity of TMOs. It was reported that suitable functional groups, which enable the strong covalent bonding between catalysts and carbon substrates, are important for the synergistic effect leading to the activity of hybrid materials.[113,114] Graphene that has two-dimensional flat structure with super-high theoretical surface area and very good electrical conductivity was found to be an ideal candidate to prepare such type of composite catalysts.

Recently, a method for one-step synthesis of Mn_3O_4/reduced graphene oxide (RGO) nanocomposites for non-aqueous Li-O_2 batteries has been developed by a LANL group,[37] as shown in **Figure 9a**. After 24 h of solvothermal reaction, monodispersed Mn_3O_4 nanoparticles were formed and uniformly bonded on the surface of RGO (**Figure 9b**). The Mn_3O_4 nanoparticles with diameters of *ca*. 4-6 nm are well crystallized (**Figure 9c**). Because the monodispersed Mn_3O_4 nanoparticles have smaller particle size compared to previously reported MnO_x-based composite, it may have a stronger interaction bonding between MnO_x and RGO, thereby leading to higher catalytic activity due to a possible synergistic effect.[102] To investigate the cathode catalyst performance, the composite was evaluated by the steady-state RDE polarization and Li-O_2 cell tests in a Li-O_2 battery with 1.0 M $LiPF_6$ in TEGDME as an electrolyte (**Figure 9d** and Figure 9e). Compared to other ratios of Mn_3O_4 and RGO, the Mn_3O_4/RGO (4:1) catalyst exhibited highest ORR activity in both half-cell and full-cell test, exhibiting an initial discharge capacity as high as 16 000 mA h g^{-1}.

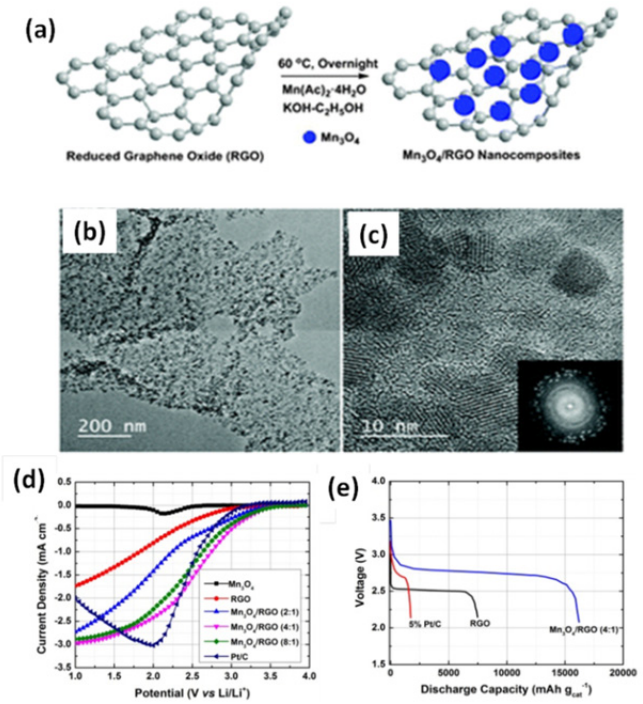

Fig. 9. (a) Schematic illustration of the one-step synthesis of Mn_3O_4/RGO nanocomposites for oxygen reduction in Li-O_2 batteries. (b, c) SEM and TEM images of the as-prepared Mn_3O_4/RGO nanocomposites with an RGO to Mn_3O_4 mass ratio of 4:1. (d) ORR steady-state RDE polarization curves for various catalysts in O_2-saturated 0.1 M $LiPF_6$ in the DME electrolyte. Rotating speed: 900 rpm; room temperature; (e) initial discharge performance of various catalysts at a current density of 50 mA g^{-1} in Li-O_2 battery tests. Reprinted with permission from Ref. 37 Copyright (2013) Royal Society of Chemistry.

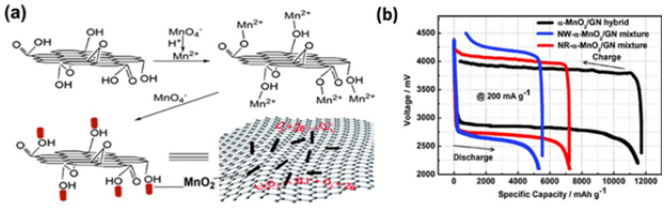

Fig. 10. (a) Schematic drawing of the growth of α-MnO_2 nanorods on GNs and the schematic structure of the α-MnO_2/GN hybrid. (b) Discharging and charging profiles of Li–O_2 batteries based on three different catalysts, α-MnO_2/GN hybrid, NW-α-MnO_2/GN mixture and NR-α-MnO_2/GN mixture. The current density and capacities were based on the mass of GNs. Reprinted with permission from Ref. 115 Copyright (2012) Royal Society of Chemistry.

Meanwhile, an α-MnO_2/RGO hybrid material has been also synthesized and employed as the catalyst for nonaqueous Li-O_2 batteries, which exhibited excellent catalytic

properties.[115] Taking advantage of the oxygen functional groups, the manganese ions were absorbed on the surface of graphene nanosheets and in-situ nucleated to grow nanorods (**Figure 10a**). This in-situ growth approach resulted in a strong covalent bonding between MnO_2 and RGO, leading to an excellent performance in Li-O_2 batteries (**Figure 10a**).

Despite of the extensive study on MnO_x-based cathode catalyst, many other transition metal oxides, such as CoO_x, FeO_x, and CuO, have been investigated in nonaqueous Li-O_2 batteries.[116-118]. Among the reported transition metal oxides, most of them exhibited relatively high catalytic ORR activity in nonaqueous Li-O_2 batteries (typically $E_{1/2}$=2.6 V versus Li^+/Li), compared to carbon-based cathode, while the OER catalytic activity vary largely between them. Ruthenium-based electrocatalysts were reported to possess relatively high catalytic activity toward OER, which is typically lower than ~4 V versus Li^+/Li, however, the high cost hampers their wide implementation in practical applications.[117,118] The alternatives for low cost but high efficiency catalysts have been actively pursued. Most recently, a ORR/OER bifunctional composite catalyst using Co_3O_4 nanofibers immobilized on oxidized graphene nanoflakes has been developed and showed highly catalytic activity for ORR/OER in a nonaqueous Li-O_2 battery.[119] The hybrid material delivered a very high initial discharge capacity of 10,500 mAh g^{-1} and a high coulombic efficiency of 88.5%. In addition, the hybrid material exhibited very good cycling stability, which stably maintained a limited capacity of 1000 mAh g^{-1} for 80 cycles without any distinctive capacity loss. The superior catalytic performance should be attributed to improved catalytic activity of 1D Co_3O_4 nanofibers with large surface area, facile electron transport via interconnected grahene nanoflakes, and fast oxygen diffusion through the highly porous matrix.

The heavy molecular weight of TMOs is another dominant factor to limit its ability to deliver higher energy density in Li-O_2 batteries. Considering this aspect on density and the concern of the accommodation of solid discharge product, porous structures with well-defined microstructure are necessary for the cathode design in Li-O_2 batteries. In doing so, mesoporous cobalt oxides (Co_3O_4) with different porosities mixed with carbon blacks were employed as the cathode catalysts in Li-O_2 batteries and demonstrated significantly improved round-trip efficiency and specific capacity over the bulk catalyst.[120] It was indicated that the highly open and continuous three-dimensional cubic mesoporous structure are imperative for the high catalytic activity.

2.3.2 Mixed metal oxide catalysts

A family of MTMOs such as perovskite $LaNiO_{3-\delta}$ and pyrochlore $Pb_2Ru_2O_{7-\delta}$, have been employed as ORR/OER catalysts in aqueous Zn-air battery systems.[121,122] Taking advantage of the knowledge learned from aqueous electrolyte, such MTMOs have attracted rising interests in the applications for nonaqueous Li-O_2 batteries.[54,81,96,97,102,123-126] In mixed transition metal oxides, some metal ion positions are substituted by other metal ions, which results in a tunable electronic structure of ORR/OER active site center and an enhanced catalytic activity.[93,109] In addition, the covalent coupling between the oxide nanoparticles and carbon substrate like carbon nanotubes and graphene usually leads to drastically improved catalytic activity. Based on these theories, a covalently coupled $MnCo_2O_4$-graphene hybrid as an oxygen cathode catalyst has been successfully developed by Dai's group at Stanford University (**Figure 11**).[49] The hybrid with controlled morphology and particle size was synthesized by direct nucleation and growth of $MnCo_2O_4$ nanoparticles on reduced graphene oxide and result in very strong covalent coupling between the oxide particles and the graphene substrate. The tuned electronic structure of active center on the oxide nanoparticles lead to a better catalytic activity than free oxide particles physically mixed with conductive carbon substrate, indicating the importance of the covalent bonding between $MnCo_2O_4$ and graphene substrate.

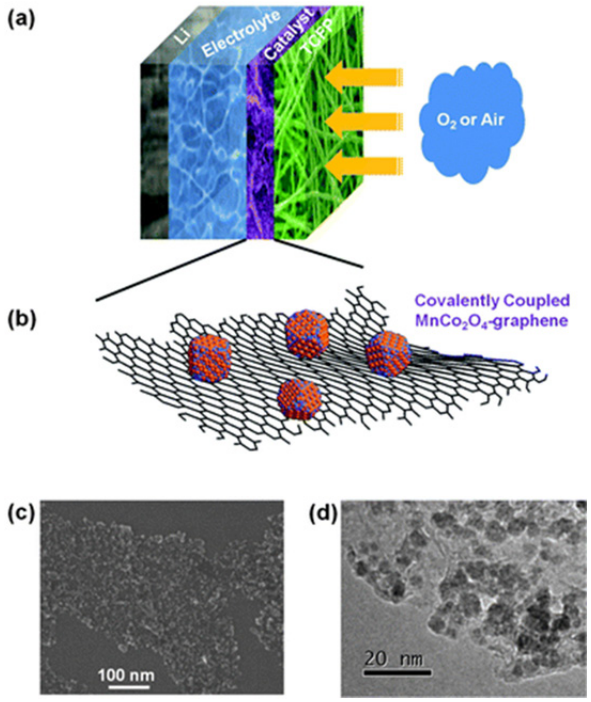

Fig. 11. $MnCo_2O_4$–graphene hybrid as a cathode catalyst for Li-O_2 batteries. (a) Schematic structure of the Li-O_2 cell catalyzed by the $MnCo_2O_4$–graphene hybrid. (b) Schematic structure of the $MnCo_2O_4$–graphene hybrid material comprised of $MnCo_2O_4$ nanoparticles covalently bonded to NGO sheets through carbon–oxygen–metal and carbon–nitrogen–metal bonds. (c) An SEM image of the $MnCo_2O_4$–graphene hybrid. (d) A TEM image of the $MnCo_2O_4$–graphene hybrid. Reprinted with permission from Ref. 49 Copyright (2012) Royal Society of Chemistry.

2.3.3 Metal nitride catalysts

Owing to their higher electronic conductivity than that of metal oxides, metal nitrides have attracted considerable interests in the development of ORR/OER catalysts and have been shown to possess very good catalytic capability in both aqueous and nonaqueous electrolyte.[98,99,127-129] To further improve their activity, metal nitrides also need to be incorporated with conductive carbon substrates, such as activated carbon, CNT or graphene. For example, a hybrid material of molybdenum nitride and N-doped carbon nanospheres (MoN/N-C) has been synthesized by hydrothermal method followed by ammonia annealing and exhibited higher ORR activity in a nonaqueous electrolyte than that of molybdenum nitride itself and the physical mixture of molybdenum nitride and N-doped carbon nanospheres.[98] Another example is that a Li-O_2 battery with TiN nanoparticles supported on Vulcan XC-72, as the cathode catalyst presented an onset potential for the OER at 2.9 V

versus Li^+/Li, which is lower than that with a mixture of micro-sized TiN and VC, and VC itself, both at 3.1 V versus Li^+/Li.[128] The enhanced performance can be ascribed to the high catalytic activity of TiN nanoparticles and the promotion of electronic conductivity by carbon combination. A similar composite of mesoporous TiN and carbon has been reported to show stable capability in catalyzing ORR/OER in Li-O_2 batteries.[130] It was found that the architectures of the bimodal porous composite were appropriate for the accommodation of a large amount of Li_2O_2 and for the efficient mass transfer of the electrolyte. Additionally, it was demonstrated that the catalyst was stable against $O_2^{\bullet-}$ and Li_2O_2 and efficient for ORR/OER comparable to Pt/C.

3. Current Challenges and Solutions

$Li–O_2$ batteries hold promise to be the next generation battery technology owing to their high specific energy. To realize the potential, it is vital to find highly active catalysts with good stability for both oxygen reduction and evolution reactions in $Li–O_2$ batteries. However, the lack of efficient catalysts and rational design of electrode structures still hampers the commercialization of this technology. Advanced ORR/OER catalysts made from earth-abundant elements with sufficient activity and stability in nonaqueous media are highly desired. Carbon composite catalysts, especially metal-free carbon catalysts, nanostructured M-N-C catalysts, and transition metal/carbon compound catalysts have received considerable attention recently as the most promising cathode catalysts in Li-O_2 batteries and have been highlighted in this review. Heteroatom doping into carbon, especially nitrogen doping with different nitrogen functionalities (pyridinic, graphitic, *etc*.), have been demonstrated to be capable of inducing ORR activity *via* structural and electronic modification of the carbon, even in Li-O_2 batteries cathodes. However, the current researches are primarily focusing on the development of ORR catalysts for Li-O_2 batteries and little has been done in exploring the OER catalysts. Therefore non-precious bifunctional electrocatalysts with low overpotential for both ORR and OER are urgently required for Li-O_2 batteries.

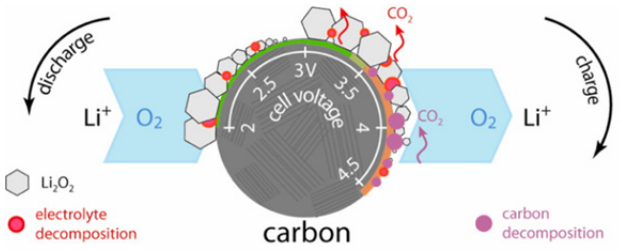

Fig. 12. Illustration of the decomposition process of carbon electrodes during discharge and charge in nonaqueous Li-O_2 batteries. Reprinted with permission from. Reprinted with permission from Ref.135 Copyright (2013) American Chemical Society.

On the other hand, the lack of stable electrolyte in nonaqueous Li-O_2 batteries is among the biggest challenge to be overcome. A large variety of electrolytes, including propylene carbonate (PC),[49] dimethoxyethane (DME),[12] tetraethylene glycol dimethyl ether (TEGDME),[19,86] dimethylformamide (DMF),[131] dimethylsulfoxide (DMSO),[1,132], tetramethylene sulfone,[133] *etc*. However, most of the studied electrolytes still suffer from rapid degradation with cycling. Recently, liquid electrolyte was replaced with a solid Li-ion conductor to circumvent the decomposition problem of liquid electrolytes, which may provide an alternative approach.[134] Besides the electrolyte, the stability of the cathode material is also a serious issue in the application of Li-O_2 batteries. So far most of the published results are obtained with carbon or carbon based cathodes. However, similar to carbon corrosion in fuel cells, carbon materials also undergo corrosion challenges at the high operation potentials, especially for the charging process and high oxygen circumstances in Li-O_2 batteries. Recently, it has been demonstrated that carbon is unstable on charging above 3.5 V in the presence of Li_2O_2, undergoing oxidative decomposition to form Li_2CO_3 (**Figure 12**).[135] Superoxide radicals generated at the cathode during discharge has also been proven to react with carbon that contains activated double bonds or aromatics to form epoxy groups and carbonates, which limits the rechargeable capability of Li-O_2 cells.[100]

Based on our current understanding of the existing catalysts, we believe that the following research directions are important to the development of highly-efficient carbon based catalysts for Li-O_2 batteries: (1) to design the catalysts with optimal distribution of macropores, mesopores, and micropores enabling efficient decomposition of discharging products; (2) to improve the catalyst stability by exploring new support materials and synthesis strategies; (3) to fundamentally understand the ORR/OER mechanisms in Li-O_2 batteries and their relationship with various catalyst active sites using both theoretical calculations (molecular/electronic level) and experimental methods.

Acknowledgements

Financial support from the Los Alamos National Laboratory Early Career Laboratory-Directed Research and Development (LDRD) Program (20110483ER) for this work is gratefully acknowledged. This research was also supported by the MSIP (Ministry of Science, ICT & Future Planning), Korea, under the C-ITRC (Convergence Information Technology Research Center) support program (NIPA-2013-H0301–13–1009) supervised by the NIPA (National IT Industry Promotion Agency).

Notes and references

[a] Materials Physics and Applications Division, Los Alamos National Laboratory, Los Alamos, New Mexico 87545, USA. E-mail: wugang@lanl.gov

[b] Interdisciplinary School of Green Energy, Ulsan National Institute of Science and Technology, Ulsan, 689-798, Korea. E-mail: jpcho@unist.ac.kr

1. Z. Q. Peng, S. A. Freunberger, Y. H. Chen and P. G. Bruce, *Science*, 2012, **337**, 563-566.
2. R. Black, B. Adams and L. F. Nazar, *Adv. Energy Mater.*, 2012, **2**, 801-815.
3. R. Cao, J. S. Lee, M. L. Liu and J. Cho, *Adv. Energy Mater.*, 2012, **2**, 816-829.
4. H. Kitaura and H. Zhou, *Adv. Energy Mater.*, 2012, **2**, 889-894.

5. G. Girishkumar, B. McCloskey, A. C. Luntz, S. Swanson and W. Wilcke, *J. Phys. Chem. Lett.*, 2010, **1**, 2193-2203.
6. P. G. Bruce, L. J. Hardwick and K. M. Abraham, *MRS Bulletin*, 2011, **36**, 506-512.
7. M. Armand and J. M. Tarascon, *Nature*, 2008, **451**, 652-657.
8. J. Wilshire and D. T. Sawyer, *Acc. Chem. Res.*, 1979, **12**, 105-110.
9. J. Hassoun, F. Croce, M. Armand and B. Scrosati, *Angew. Chem. Int. Ed.*, 2011, **50**, 2999-3002.
10. M. M. Islam, T. Imase, T. Okajima, M. Takahashi, Y. Niikura, N. Kawashima, Y. Nakamura and T. Ohsaka, *J. Phys. Chem. A*, 2009, **113**, 912-916.
11. S. A. Freunberger, Y. H. Chen, N. E. Drewett, L. J. Hardwick, F. Barde and P. G. Bruce, *Angew. Chem. Int. Ed.*, 2011, **50**, 8609-8613.
12. B. D. McCloskey, D. S. Bethune, R. M. Shelby, G. Girishkumar and A. C. Luntz, *J. Phys. Chem. Lett.*, 2011, **2**, 1161-1166.
13. S. A. Freunberger, Y. H. Chen, Z. Q. Peng, J. M. Griffin, L. J. Hardwick, F. Barde, P. Novak and P. G. Bruce, *J. Am. Chem. Soc.*, 2011, **133**, 8040-8047.
14. W. Xu, K. Xu, V. V. Viswanathan, S. A. Towne, J. S. Hardy, J. Xiao, D. H. Hu, D. Y. Wang and J. G. Zhang, *J. Power Sources*, 2011, **196**, 9631-9639.
15. R. R. Mitchell, B. M. Gallant, C. V. Thompson and Y. Shao-Horn, *Energy Environ. Sci.*, 2011, **4**, 2952-2958.
16. Y. Shao, S. Park, J. Xiao, J.-G. Zhang, Y. Wang and J. Liu, *ACS Catal.*, 2012, **2**, 844-857.
17. R. Black, J.-H. Lee, B. Adams, C. A. Mims and L. F. Nazar, *Angew. Chem. Int. Ed.*, 2013, **125**, 410-414.
18. B. D. McCloskey, R. Scheffler, A. Speidel, D. S. Bethune, R. M. Shelby and A. C. Luntz, *J. Am. Chem. Soc.*, 2011, **133**, 18038-18041.
19. G. Wu, N. H. Mack, W. Gao, S. G. Ma, R. Q. Zhong, J. T. Han, J. K. Baldwin and P. Zelenay, *ACS Nano*, 2012, **6**, 9764-9776.
20. Q. Li, P. Xu, W. Gao, S. Ma, G. Zhang, R. Cao, J. Cho, H.-L. Wang and G. Wu, *Adv. Mater.*, 2014, **26**, 1378-1386.
21. B. D. McCloskey, D. S. Bethune, R. M. Shelby, T. Mori, R. Scheffler, A. Speidel, M. Sherwood and A. C. Luntz, *J. Phys. Chem. Lett.*, 2012, **3**, 3043-3047.
22. A. Debart, A. J. Paterson, J. Bao and P. G. Bruce, *Angew. Chem. Int. Ed.*, 2008, **47**, 4521-4524.
23. Y. C. Lu, Z. C. Xu, H. A. Gasteiger, S. Chen, K. Hamad-Schifferli and Y. Shao-Horn, *J. Am. Chem. Soc.*, 2010, **132**, 12170-12171.
24. J. Xiao, D. Mei, X. Li, W. Xu, D. Wang, G. L. Graff, W. D. Bennett, Z. Nie, L. V. Saraf, I. A. Aksay, J. Liu and J.-G. Zhang, *Nano Lett.*, 2011, **11**, 5071-5078.
25. F. Jaouen, E. Proietti, M. Lefevre, R. Chenitz, J. P. Dodelet, G. Wu, H. T. Chung, C. M. Johnston and P. Zelenay, *Energy Environ. Sci.*, 2011, **4**, 114-130.
26. J. Suntivich, K. J. May, H. A. Gasteiger, J. B. Goodenough and Y. Shao-Horn, *Science*, 2011, **334**, 1383-1385.
27. Q. Li, P. Xu, B. Zhang, G. Wu, H. T. Zhao, E. G. Fu and H. L. Wang, *Nanoscale*, 2013, **5**, 7397-7402.
28. C. C. L. McCrory, S. H. Jung, J. C. Peters and T. F. Jaramillo, *J. Am. Chem. Soc.*, 2013, **135**, 16977-16987.
29. J. J. Xu, Z. L. Wang, D. Xu, L. L. Zhang and X. B. Zhang, *Nat. Commun.*, 2013, **4**.
30. A. Rabis, P. Rodriguez and T. J. Schmidt, *ACS Catal.*, 2012, **2**, 864-890.
31. Z. Chen, D. Higgins, A. Yu, L. Zhang and J. Zhang, *Energy Environ. Sci.*, 2011, **4**, 3167-3192.
32. G. Wu, G. Cui, D. Li, P.-K. Shen and N. Li, *J. Mater. Chem.*, 2009, **19**, 6581-6589.
33. Q. Li, R. Cao, J. Cho and G. Wu, *Adv. Energy Mater.*, 2013, doi:aenm.201301415.
34. G. Wu, K. L. More, C. M. Johnston and P. Zelenay, *Science*, 2011, **332**, 443-447.
35. G. Wu, M. A. Nelson, N. H. Mack, S. G. Ma, P. Sekhar, F. H. Garzon and P. Zelenay, *Chem. Commun.*, 2010, **46**, 7489-7491.
36. G. Wu and P. Zelenay, *Acc. Chem. Res.*, 2013, **46**, 1878-1889.
37. Q. Li, P. Xu, B. Zhang, H. Tsai, J. Wang, H.-L. Wang and G. Wu, *Chem. Commun.*, 2013, **49**, 10838-10840.
38. G. Wu, M. Nelson, S. Ma, H. Meng, G. Cui and P. K. Shen, *Carbon*, 2011, **49**, 3972-3982.
39. Q. G. He, Q. Li, S. Khene, X. M. Ren, F. E. Lopez-Suarez, D. Lozano-Castello, A. Bueno-Lopez and G. Wu, *J. Phys. Chem. C*, 2013, **117**, 8697-8707.
40. Q. Li, P. Xu, B. Zhang, H. Tsai, S. Zheng, G. Wu and H.-L. Wang, *J. Phys. Chem. C*, 2013, **117**, 13872-13878.
41. G. Wu, C. M. Johnston, N. H. Mack, K. Artyushkova, M. Ferrandon, M. Nelson, J. S. Lezama-Pacheco, S. D. Conradson, K. L. More, D. J. Myers and P. Zelenay, *J. Mater. Chem.*, 2011, **21**, 11392-11405.
42. G. Wu, K. L. More, P. Xu, H. L. Wang, M. Ferrandon, A. J. Kropf, D. J. Myers, S. G. Ma, C. M. Johnston and P. Zelenay, *Chem. Commun.*, 2013, **49**, 3291-3293.
43. N. P. Subramanian, X. Li, V. Nallathambi, S. P. Kumaraguru, H. Colon-Mercado, G. Wu, J.-W. Lee and B. N. Popov, *J. Power Sources*, 2009, **188**, 38-44.
44. V. Nallathambi, J.-W. Lee, S. P. Kumaraguru, G. Wu and B. N. Popov, *J. Power Sources*, 2008, **183**, 34-42.
45. K. Parvez, S. Yang, Y. Hernandez, A. Winter, A. Turchanin, X. Feng and K. Müllen, *ACS Nano*, 2012.
46. L. Qu, Y. Liu, J.-B. Baek and L. Dai, *ACS Nano*, 2010, **4**, 1321-1326.
47. H. R. Byon, J. Suntivich and Y. Shao-Horn, *Chem. Mater.*, 2011, **23**, 3421-3428.
48. L. Lai, J. R. Potts, D. Zhan, L. Wang, C. K. Poh, C. Tang, H. Gong, Z. Shen, J. Lin and R. S. Ruoff, *Energy Environ. Sci.*, 2012, **5**, 7936-7942.
49. H. L. Wang, Y. Yang, Y. Y. Liang, G. Y. Zheng, Y. G. Li, Y. Cui and H. J. Dai, *Energy Environ. Sci.*, 2012, **5**, 7931-7935.
50. Y. Li, W. Zhou, H. Wang, L. Xie, Y. Liang, F. Wei, J.-C. Idrobo, S. J. Pennycook and H. Dai, *Nat. Nanotechnol.*, 2012, **7**, 394-400.
51. J. L. Shui, N. K. Karan, M. Balasubramanian, S. Y. Li and D. J. Liu, *J. Am. Chem. Soc.*, 2012, **134**, 16654-16661.
52. V. Nallathambi, G. Wu, N. Subramanian, S. Kumaraguru, J.-W. Lee and B. Popov, *ECS Trans.*, 2007, **11**, 241-247.
53. R. Cao, R. Thapa, H. Kim, X. Xu, M. G. Kim, Q. Li, N. Park, M. L. Liu and J. Cho, *Nat. Commun.*, 2013, **4**.
54. Y. Y. Shao, F. Ding, J. Xiao, J. Zhang, W. Xu, S. Park, J. G. Zhang, Y. Wang and J. Liu, *Adv. Func. Mater.*, 2013, **23**, 987-1004.
55. G. Wu, C. Dai, D. Wang, D. Li and N. Li, *J. Mater. Chem.*, 2010, **20**, 3059-3068.
56. K. M. Abraham and Z. Jiang, *J. Electrochem. Soc.*, 1996, **143**, 1-5.
57. J. Xiao, D. H. Wang, W. Xu, D. Y. Wang, R. E. Williford, J. Liu and J. G. Zhang, *J. Electrochem. Soc.*, 2010, **157**, A487-A492.

58. J. Read, K. Mutolo, M. Ervin, W. Behl, J. Wolfenstine, A. Driedger and D. Foster, *J. Electrochem. Soc.*, 2003, **150**, A1351-A1356.
59. T. Kuboki, T. Okuyama, T. Ohsaki and N. Takami, *J. Power Sources*, 2005, **146**, 766-769.
60. W. Xu, J. Xiao, J. Zhang, D. Y. Wang and J. G. Zhang, *J. Electrochem. Soc.*, 2009, **156**, A773-A779.
61. P. Albertus, G. Girishkumar, B. McCloskey, R. S. Sanchez-Carrera, B. Kozinsky, J. Christensen and A. C. Luntz, *J. Electrochem. Soc.*, 2011, **158**, A343-A351.
62. J. Read, *J. Electrochem. Soc.*, 2002, **149**, A1190-A1195.
63. S. S. Zhang, D. Foster and J. Read, *J. Power Sources*, 2010, **195**, 1235-1240.
64. Y. Shao, S. Zhang, M. H. Engelhard, G. Li, G. Shao, Y. Wang, J. Liu, I. A. Aksay and Y. Lin, *J. Mater. Chem.*, 2010, **20**, 7491-7496.
65. C. Z. Zhu and S. J. Dong, *Nanoscale*, 2013, **5**, 1753-1767.
66. Y. L. Li, J. J. Wang, X. F. Li, D. S. Geng, R. Y. Li and X. L. Sun, *Chem. Commun.*, 2011, **47**, 9438-9440.
67. B. Sun, B. Wang, D. W. Su, L. D. Xiao, H. Ahn and G. X. Wang, *Carbon*, 2012, **50**, 727-733.
68. E. Yoo and H. S. Zhou, *ACS Nano*, 2011, **5**, 3020-3026.
69. G. Wu, D. Y. Li, C. S. Dai, D. L. Wang and N. Li, *Langmuir*, 2008, **24**, 3566-3575.
70. S. Maldonado and K. J. Stevenson, *J. Phys. Chem. B*, 2005, **109**, 4707-4716.
71. S. U. Lee, R. V. Belosludov, H. Mizuseki and Y. Kawazoe, *Small*, 2009, **5**, 1769-1775.
72. Y. L. Li, J. J. Wang, X. F. Li, J. Liu, D. S. Geng, J. L. Yang, R. Y. Li and X. L. Sun, *Electrochem. Commun.*, 2011, **13**, 668-672.
73. Y. L. Li, J. J. Wang, X. F. Li, D. S. Geng, M. N. Banis, R. Y. Li and X. L. Sun, *Electrochem. Commun.*, 2012, **18**, 12-15.
74. K. P. Gong, F. Du, Z. H. Xia, M. Durstock and L. M. Dai, *Science*, 2009, **323**, 760-764.
75. K. Wiesener, *Electrochim. Acta*, 1986, **31**, 1073-1078.
76. R. Jasinski, *Nature*, 1964, **201**, 1212-1214.
77. S. Gupta, D. Tryk, I. Bae, W. Aldred and E. Yeager, *J. Appl. Electrochem.*, 1989, **19**, 19-27.
78. M. Lefevre, E. Proietti, F. Jaouen and J. P. Dodelet, *Science*, 2009, **324**, 71-74.
79. H. T. Chung, J. H. Won and P. Zelenay, *Nat. Commun.*, 2013, **4**, 1922.
80. E. Proietti, F. Jaouen, M. Lefevre, N. Larouche, J. Tian, J. Herranz and J. P. Dodelet, *Nat. Commun.*, 2011, **2**, 416.
81. M. Ferrandon, A. J. Kropf, D. J. Myers, K. Artyushkova, U. Kramm, P. Bogdanoff, G. Wu, C. M. Johnston and P. Zelenay, *J. Phys. Chem. C*, 2012, **116**, 16001-16013.
82. M. Ferrandon, X. Wang, A. J. Kropf, D. J. Myers, G. Wu, C. M. Johnston and P. Zelenay, *Electrochim. Acta*, 2013, **110**, 282-291.
83. D. Ohms, S. Herzog, R. Franke, V. Neumann, K. Wiesener, S. Gamburcev, A. Kaisheva and I. Iliev, *J. Power Sources*, 1992, **38**, 327-334.
84. X. G. Fu, Y. R. Liu, X. P. Cao, J. T. Jin, Q. Liu and J. Y. Zhang, *Appl. Catal. B Environ.*, 2013, **130**, 143-151.
85. H. T. Chung, C. M. Johnston, K. Artyushkova, M. Ferrandon, D. J. Myers and P. Zelenay, *Electrochem. Commun.*, 2010, **12**, 1792-1795.
86. L. Trahey, N. K. Karan, M. K. Y. Chan, J. Lu, Y. Ren, J. Greeley, M. Balasubramanian, A. K. Burrell, L. A. Curtiss and M. M. Thackeray, *Adv. Energy Mater.*, 2013, **3**, 75-84.
87. X. G. Li, B. N. Popov, T. Kawahara and H. Yanagi, *J. Power Sources*, 2011, **196**, 1717-1722.
88. J. S. Lee, G. S. Park, S. T. Kim, M. L. Liu and J. Cho, *Angew. Chem. Int. Ed.*, 2013, **52**, 1026-1030.
89. C. O. Laoire, S. Mukerjee, K. M. Abraham, E. J. Plichta and M. A. Hendrickson, *J. Phys. Chem. C*, 2010, **114**, 9178-9186.
90. A. Morozan and F. Jaouen, *Energy Environ. Sci.*, 2012, **5**, 9269-9290.
91. P. G. Bruce, S. A. Freunberger, L. J. Hardwick and J. M. Tarascon, *Nat. Mater.*, 2012, **11**, 19-29.
92. J.-S. Lee, S. Tai Kim, R. Cao, N.-S. Choi, M. Liu, K. T. Lee and J. Cho, *Adv. Energy Mater.*, 2011, **1**, 34-50.
93. F. Cheng and J. Chen, *Chem. Soc. Rev.*, 2012, **41**, 2172-2192.
94. L. Trahey, C. S. Johnson, J. T. Vaughey, S.-H. Kang, L. J. Hardwick, S. A. Freunberger, P. G. Bruce and M. M. Thackeray, *Electrochem. Solid-State Lett.*, 2011, **14**, A64-A66.
95. Y. Zhao, L. Xu, L. Mai, C. Han, Q. An, X. Xu, X. Liu and Q. Zhang, *Pro. Nat. Aca. Sci.*, 2012, **109**, 19569-19574.
96. A. Grimaud, C. E. Carlton, M. Risch, W. T. Hong, K. J. May and Y. Shao-Horn, *J. Phys. Chem. C*, 2013, **117**, 25926-25932.
97. K.-N. Jung, J.-I. Lee, W. B. Im, S. Yoon, K.-H. Shin and J.-W. Lee, *Chem. Commun.*, 2012, **48**, 9406-9408.
98. K. Zhang, L. Zhang, X. Chen, X. He, X. Wang, S. Dong, L. Gu, Z. Liu, C. Huang and G. Cui, *ACS Appl. Mater. Interfaces*, 2013, **5**, 3677-3682.
99. L. Zhang, X. Zhang, Z. Wang, J. Xu, D. Xu and L. Wang, *Chem. Commun.*, 2012, **48**, 7598-7600.
100. D. M. Itkis, D. A. Semenenko, E. Y. Kataev, A. I. Belova, V. S. Neudachina, A. P. Sirotina, M. Hävecker, D. Teschner, A. Knop-Gericke, P. Dudin, A. Barinov, E. A. Goodilin, Y. Shao-Horn and L. V. Yashina, *Nano Lett.*, 2013, **13**, 4697-4701.
101. M. M. Ottakam Thotiyl, S. A. Freunberger, Z. Peng and P. G. Bruce, *J. Am. Chem. Soc.*, 2012, **135**, 494-500.
102. H. Wang and H. Dai, *Chem. Soc. Rev.*, 2013, **42**, 3088-3113.
103. C. Kavakli, S. Meini, G. Harzer, N. Tsiouvaras, M. Piana, A. Siebel, A. Garsuch, H. A. Gasteiger and J. Herranz, *ChemCatChem*, 2013, **5**, 3358-3373.
104. G. Q. Zhang, J. P. Zheng, R. Liang, C. Zhang, B. Wang, M. Au, M. Hendrickson and E. J. Plichta, *J. Electrochem. Soc.*, 2011, **158**, A822-A827.
105. Y. Cao, Z. Wei, J. He, J. Zang, Q. Zhang, M. Zheng and Q. Dong, *Energy Environ. Sci.*, 2012, **5**, 9765-9768.
106. D. Oh, J. Qi, Y.-C. Lu, Y. Zhang, Y. Shao-Horn and A. M. Belcher, *Nat. Commun.*, 2013, **4**, 2756.
107. Q. C. Liu, J. J. Xu, Z. W. Chang and X. B. Zhang, *J. Mater. Chem. A*, 2014, DOI: 10.1039/C1033TA14011C
108. L. L. Zhang, X. B. Zhang, Z. L. Wang, J. J. Xu, D. Xu and L. M. Wang, *Chem. Commun.*, 2012, **48**, 7598-7600.
109. Z. L. Wang, D. Xu, J. J. Xu, L. L. Zhang and X. B. Zhang, *Adv. Func. Mater.*, 2012, **22**, 3699-3705.
110. M. Casas-Cabanas, G. Binotto, D. Larcher, A. Lecup, V. Giordani and J. M. Tarascon, *Chem. Mater.*, 2009, **21**, 1939-1947.
111. F. Cheng, T. Zhang, Y. Zhang, J. Du, X. Han and J. Chen, *Angew. Chem. Int. Ed.*, 2013, **52**, 2474-2477.
112. J.-H. Lee, R. Black, G. Popov, E. Pomerantseva, F. Nan, G. A. Botton and L. F. Nazar, *Energy Environ. Sci.*, 2012, **5**, 9558-9565.
113. Y. Liang, Y. Li, H. Wang, J. Zhou, J. Wang, T. Regier and H. Dai, *Nat. Mater.*, 2011, **10**, 780-786.

114. G. Xia, N. Li, D. Li, R. Liu, C. Wang, Q. Li, X. Lü, J. S. Spendelow, J. Zhang and G. Wu, *ACS Appl. Mater. Interfaces*, 2013, **5**, 8607-8614.
115. Y. Cao, Z. Wei, J. He, J. Zang, Q. Zhang, M. Zheng and Q. Dong, *Energy & Environmental Science*, 2012, **5**, 9765-9768.
116. A. Débart, J. Bao, G. Armstrong and P. G. Bruce, *J. Power Sources*, 2007, **174**, 1177-1182.
117. H.-G. Jung, Y. S. Jeong, J.-B. Park, Y.-K. Sun, B. Scrosati and Y. J. Lee, *ACS Nano*, 2013, **7**, 3532-3539.
118. E. Yilmaz, C. Yogi, K. Yamanaka, T. Ohta and H. R. Byon, *Nano Lett.*, 2013, **13**, 4679-4684.
119. W.-H. Ryu, T.-H. Yoon, S. H. Song, S. Jeon, Y.-J. Park and I.-D. Kim, *Nano Lett.*, 2013, **13**, 4190-4197.
120. Y. Cui, Z. Wen, S. Sun, Y. Lu and J. Jin, *Solid State Ionics*, 2012, **225**, 598-603.
121. H. S. Horowitz, J. M. Longo and H. H. Horowitz, *J. Electrochem. Soc.*, 1983, **130**, 1851-1859.
122. J. B. Goodenough, R. Manoharan and M. Paranthaman, *J. Am. Chem. Soc.*, 1990, **112**, 2076-2082.
123. K. P. C. Yao, D. G. Kwabi, R. A. Quinlan, A. N. Mansour, A. Grimaud, Y.-L. Lee, Y.-C. Lu and Y. Shao-Horn, *J. Electrochem. Soc.*, 2013, **160**, A824-A831.
124. S. H. Oh, R. Black, E. Pomerantseva, J.-H. Lee and L. F. Nazar, *Nat. Chem.*, 2012, **4**, 1004-1010.
125. J. J. Xu, D. Xu, Z. L. Wang, H. G. Wang, L. L. Zhang and X. B. Zhang, *Angew. Chem. Int. Ed.*, 2013, **52**, 3887-3890.
126. J. J. Xu, Z. L. Wang, D. Xu, F. Z. Meng and X. B. Zhang, *Energy Environ. Sci.*, 2014, DOI: 10.1039/C1033EE42934B
127. H. Wu and W. Chen, *J. Am. Chem. Soc.*, 2011, **133**, 15236-15239.
128. F. Li, R. Ohnishi, Y. Yamada, J. Kubota, K. Domen, A. Yamada and H. Zhou, *Chem. Commun.*, 2013, **49**, 1175-1177.
129. S. Dong, X. Chen, S. Wang, L. Gu, L. Zhang, X. Wang, X. Zhou, Z. Liu, P. Han, Y. Duan, H. Xu, J. Yao, C. Zhang, K. Zhang, G. Cui and L. Chen, *ChemSusChem*, 2012, **5**, 1712-1715.
130. J. Park, Y.-S. Jun, W.-R. Lee, J. A. Gerbec, K. A. See and G. D. Stucky, *Chem. Mater.*, 2013, **25**, 3779-3781.
131. Y. Chen, S. A. Freunberger, Z. Peng, F. Barde and P. G. Bruce, *J. Am. Chem. Soc.*, 2012, **134**, 7952-7957.
132. D. Xu, Z. L. Wang, J. J. Xu, L. L. Zhang and X. B. Zhang, *Chem. Commun.*, 2012, **48**, 6948-6950.
133. D. Xu, Z. L. Wang, J. J. Xu, L. L. Zhang, L. M. Wang and X. B. Zhang, *Chem. Commun.*, 2012, **48**, 11674-11676.
134. T. Zhang and H. S. Zhou, *Nat. Commun.*, 2013, **4**, 1817.
135. M. M. O. Thotiyl, S. A. Freunberger, Z. Q. Peng and P. G. Bruce, *J. Am. Chem. Soc.*, 2013, **135**, 494-500.

Table of Content

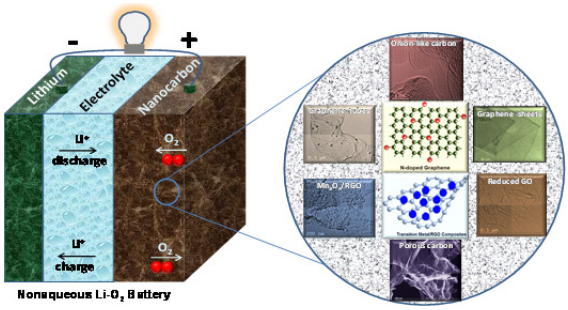

Structure-activity correlations for nanocarbon oxygen cathode catalysts in nonaqueous Li-O_2 batteries are discussed, providing guidance for rational catalyst design.

Qing Li is a postdoctoral research associate at Los Alamos National Laboratory. He received his BSc from Wuhan University in 2005 and his Ph.D. from Peking University in 2010, both in chemistry. His research interests include functional nanomaterials and their applications in PEM fuel cells, metal-air batteries, and biosensors.

Ruiguo Cao received his Ph.D degree in Physical Chemistry at Peking University, China (2010). He was a postdoctoral researcher in the Interdisciplinary School of Green Energy at Ulsan National Institute of Science and Technology, Korea. Currently, he is a postdoctoral research associate at Pacific Northwest National Laboratory. His research mainly focuses on the design and synthesis of ORR catalysts for metal air batteries, including Zn-air and Li-air batteries.

Jaephil Cho is a professor and dean in Interdisciplinary School of Green Energy at UNIST (Korea). He is a director of Converging Research Center for Innovative Battery Technologies (granted by Ministry of Education,Science & Technology of in Korea) and of IT Research Center (granted by Ministry of Knowledge Economy in Korea). His current research is focused mainly on Li-ion and Zn-Air batteries and nanomaterials for energy storage.

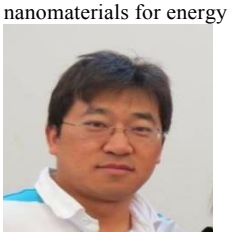

Gang Wu is a scientist at Los Alamos National Laboratory (LANL). He completed his Ph.D. studies in 2004 at the Harbin Institute of Technology, concentrating on electrodeposition and electrocatalysis. After postdoctoral trainings at Tsinghua University (2004-2006), the University of South Carolina (2006-2008), and LANL (2008-2010), he became a research scientist at LANL in 2010. Wu is an electrochemist and materials scientist and has authored or coauthored more than 90 papers in the areas of nanostructured catalysts and electrode materials for electrochemical energy storage and conversion technologies (*e.g.*, polymer electrolyte fuel cells, metal-air batteries, and lithium ion batteries).